Single-Molecule Study of Protein−Protein Interaction Dynamics in a Cell Signaling System

Xin Tan,[†] Perihan Nalbant,[‡] Alexei Toutchkine,[‡] Dehong Hu,[†] Erich R. Vorpagel,[†] Klaus M. Hahn,[‡] and H. Peter Lu*[,†]

Fundamental Science Division, Pacific Northwest National Laboratory, P.O. Box 999, MSIN K8-88, Richland, Washington 99352, and Department of Cell Biology, The Scripps Research Institute, La Jolla, California 92037

Received: May 23, 2003; In Final Form: August 22, 2003

We report a study on protein−protein noncovalent interactions in an intracellular signaling protein complex, using single-molecule spectroscopy and molecular dynamics (MD) simulations. A Wiskott−Aldrich Syndrome Protein (WASP) fragment that binds only the activated intracellular signaling protein Cdc42 was labeled with a novel solvatochromic dye and used to probe hydrophobic interactions significant to Cdc42/WASP recognition. The study shows static and dynamic inhomogeneous conformational fluctuations of the protein complex that involve bound and loosely bound states. A two-coupled, two-state Markovian kinetic model is proposed for the conformational dynamics. The MD simulations explore the origin of these conformational states and associated conformational fluctuations in this protein−protein interaction system.

Introduction

Cell signaling is at the core of most biological functions and often involves dynamic interactions among proteins. Protein−protein interactions induce conformational changes that initiate chain reactions, which, in turn, lead to cellular responses. A comprehensive characterization of such protein interactions is critical to understanding the regulatory mechanisms that control cellular functions.

To study protein interactions in cell signaling, ensemble measurements, which yield information only on averaged properties, are inadequate. The crucial early events of cell signaling often involve only a few molecules and then are magnified along the signaling pathways. Furthermore, for intrinsically heterogeneous systems such as protein complexes, protein interaction dynamics possess both spatial and temporal inhomogeneities,[1−8] which result in inhomogeneous rates among protein complexes (static inhomogeneity) and rate fluctuations during the time of protein−protein interaction (dynamic inhomogeneity).

Under physiological conditions, it is difficult for ensemble-averaged experiments[9] to identify and characterize static inhomogeneity; moreover, it is almost impossible for such experiments to identify dynamic inhomogeneity or distinguish between the two inhomogeneities; stochastic protein−protein interactions prevent such characterizations when many molecules are measured simultaneously. Single-molecule spectroscopy is powerful in regard to obtaining such information, because it is capable of characterizing biomolecular processes that are inhomogeneous and unsynchronizable.[10−18] The high temporal and spatial resolution obtainable in single-molecule fluorescence spectroscopy[13−18] makes it ideal for studying conformational dynamics and localization of proteins under physiological conditions.

We recently demonstrated the application of single-molecule fluorescence spectroscopy to DNA−protein interactions in DNA damage recognition.[16] Large-amplitude conformational fluctuations were observed that underlie significant static and dynamic inhomogeneities in the interactions of DNA−protein complexes, which suggests that biomolecular recognition involves a highly flexible protein tertiary structure. This finding, which is in agreement with recent NMR structural studies of protein complexes, indicates that binding domains undergo dramatic conformational changes from disordered to ordered states upon complex formation.[19,20] It is possible that structural transitions of flexible conformational domains are common in biomolecular recognition, which can be identified by measuring single-molecule conformational fluctuation dynamics.

In the current study, the interactions of an intracellular signaling protein Cdc42 with its downstream effector protein, Wiskott−Aldrich Syndrome Protein (WASP), were examined using single-molecule fluorescence spectroscopy. Cdc42 belongs to the Rho family of small GTP-binding proteins (GTPases) that act as molecular switches in signaling pathways to regulate diverse cellular responses.[21,22] Only when it is bound to guanosine 5′-triphosphate (GTP) does Cdc42 assume an active conformation that enables it to bind and activate a series of effector proteins via direct protein−protein noncovalent interactions. Previous solution NMR and X-ray crystallographic analyses[19,20,22,23] and studies of binding energetics[20,24,25] provided a knowledge base to facilitate our interpretation of the single-molecule data.

Materials and Methods

We used a dye-labeled fragment of WASP (denoted CBD, for the Cdc42 binding domain of WASP) to track Cdc42 activity and protein−protein interactions in the binding complex. CBD, which is a 13-kDa WASP fragment (residues 201−320), contains the CRIB (Cdc42/RAC interactive binding) motif (238−251), an N-terminal portion (201−237), and a C-terminal segment (252−320), with dye labeling at residue 271 via a cysteine mutation. This biosensor was designed for live-cell imaging based upon a domain-dye approach that is advantageous for studying unlabeled proteins *in vivo*, and a novel solvatochromic dye, I-SO (indolenine-benzothiophen-3-one-1,1-di-

* Author to whom correspondence should be addressed. E-mail: peter.lu@pnl.gov.
[†] Pacific Northwest National Laboratory.
[‡] The Scripps Research Institute.

10.1021/jp0306491 CCC: $27.50
Published on Web 12/09/2003

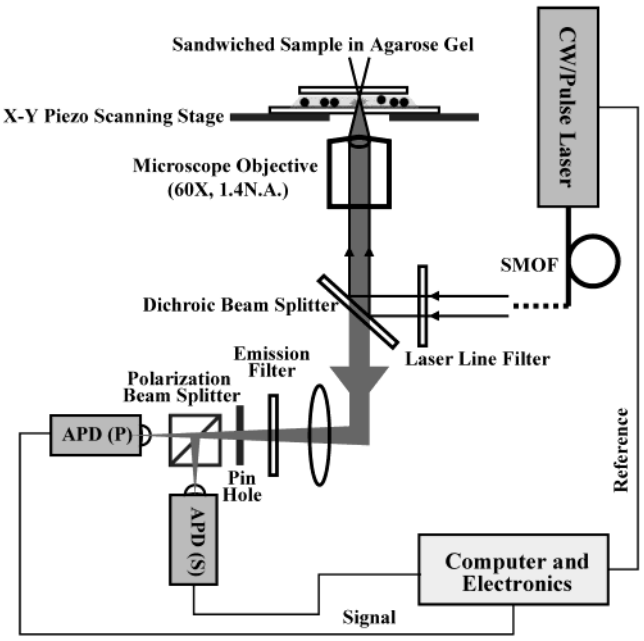

Figure 1. Instrumentation for single-molecule fluorescence experiments. Single-molecule measurements were performed on an inverted confocal fluorescence microscope (Nikon model Diaphot 300) with excitation light from a continuous-wave (CW) or pulsed laser source. Individual protein complexes embedded in agarose gel were located by raster-scanning the sample. Fluorescence photons were directed onto avalanche photodiodes (APDs) to acquire emission images and time trajectories.

oxide), whose fluorescence properties are sensitive to changes in the local environment.[26−28]

For ensemble-averaged fluorescence measurements, assays were prepared by a 1:1 volume-ratio mixing of CBD (300 nM) and Cdc42 (1 μM) loaded with GTP or guanosine 5′-diphosphate (GDP, 10 μM) in buffer solutions (50 mM *tris*-HCl, pH 7.6, 50 mM NaCl, 5 mM $MgCl_2$, 1mM DTT). Steady-state ensemble fluorescence measurements were performed on a fluorometer (PTI QM-2000). For the single-molecule experiments, Cdc42−CBD protein complexes at nanomolar concentrations were embedded in agarose gel (0.5%) and sandwiched between two cleaned cover glasses.

Single-molecule measurements were performed on an inverted confocal fluorescence microscope (Nikon model Diaphot 300) under ambient conditions.[16,29] Figure 1 shows the schematics of the experimental setup. A continuous-wave (CW) krypton-ion laser (Innova 90C, Coherent) or a Nd:YAG pumped picosecond-pulsed R6G dye laser (Coherent) delivered the 568-nm excitation light via a single-mode optical fiber (SMOF). The linear polarized light was focused to a near diffraction-limited spot in the sample by a high numerical aperture objective (60×, N.A. = 1.4, Nikon). Individual protein complexes were located by raster-scanning the sample. Fluorescence photons were directed onto one or two silicon avalanche photodiodes (APDs), to acquire emission images and time trajectories from single-protein complexes. For single-molecule anisotropy experiments, a polarization beam-splitter cube (CVI Laser) was used to separate the two orthogonal polarization components into two APD detectors. Fluorescence time-stamping TCSPC (time-correlated single-photon counting)[29−31] data were collected using a PicoQuant TimeHarp 200 card in a time-tagged time-resolved (T3R) mode.

The molecular dynamics (MD) simulations were performed on an SGI Onyx2 super-computer, using Insight II software (Accelrys, Inc.). Energy minimization was performed using a molecular mechanics CVFF force field.[32,33] MD trajectories were calculated after energy minimization with a distance-dependent dielectric constant.[32,34]

Results and Discussion

The ensemble-averaged fluorescence measurements of the dye and protein assay are summarized in Figure 2. It clearly demonstrates the binding activity of the dye-labeled CBD biosensor system and its sensitivity to the environmental hydrophobicity. The results are consistent with a previous report.[27] Figure 2A shows the fluorescence emission spectra of the solvatochromic dye I−SO in water, methanol, and butanol. The dye fluorescence intensity increased by ∼3-fold as the solvent hydrophobicity increased from water to methanol and butanol. We also observed a solvent-dependent change in the dye fluorescence lifetimes, from ∼200 ps in water to ∼1 ns in more-hydrophobic solvents such as methanol, in ensemble-averaged TCSPC measurements.

Figure 2B shows the result of a control fluorescence assay experiment. Upon binding of the dye-labeled CBD biosensor to the activated GTP-loaded Cdc42, fluorescence intensity increased by a factor of 2−3 as the dye molecule probed the hydrophobic interface of the protein−protein interactions.[19,24] In contrast, the GDP-loaded Cdc42 did not yield such an intensity change, because Cdc42 was not activated by GDP and was incapable of binding to the CBD biosensor.[27] The dye-labeled CBD alone in buffer solution gave only low fluorescence intensity, suggesting that CBD alone, without a protein−protein interaction interface, does not provide a hydrophobic environment for the dye molecule. The attached I−SO dye is sensitive only to active binding of Cdc42−CBD that forms a hydrophobic interface accessible to or around the dye molecule. Our MD simulations discussed later have further illustrated the dye's local environment and the interface structure of the protein−protein interactions. In our experiments, a nonhydrolyzable GTP analogue, GTP-γ-S, was used to irreversibly bind and lock Cdc42 in the active conformation.[27] Thus, the GTP binding and unbinding process was eliminated from the single-molecule experiments that measured only the activated Cdc42 interacting with CBD. The effects of GTP-γ-S are the same as that of GTP, and the biological relevance and validity of using GTP-γ-S has been well established in the literature.[26]

The low fluorescence intensity of dye-labeled CBD alone gives the advantage of eliminating signal contamination in the single-molecule protein−protein interaction experiments. We have studied individual CBD molecules without the presence of Cdc42 in buffer and agarose gel, and we found that the single molecules of dye-labeled CBD alone were not detectable beyond the background noise, because of low fluorescence intensity. Therefore, the single molecules being probed are almost exclusively the Cdc42−CBD complexes, which is consistent with the ensemble-averaged control results (see Figure 2).

Previous NMR analyses have indicated that the WASP fragments undergo dramatic conformational changes from disordered to ordered tertiary structures in the presence of the GTP-activated Cdc42.[19,20] Preferential binding of WASP to GTP-activated Cdc42 seems to be derived not only from polar and hydrophobic contacts involving highly conserved residues in the CRIB (Cdc42/RAC interactive binding) motif but also from hydrophobic interactions outside the CRIB motif.[19,20,35] In the present study, the dye molecule was intended to probe the extra-CRIB hydrophobic interactions significant to Cdc42/WASP recognition. As shown in the inset of Figure 2B, the dye molecule was strategically attached to a site among

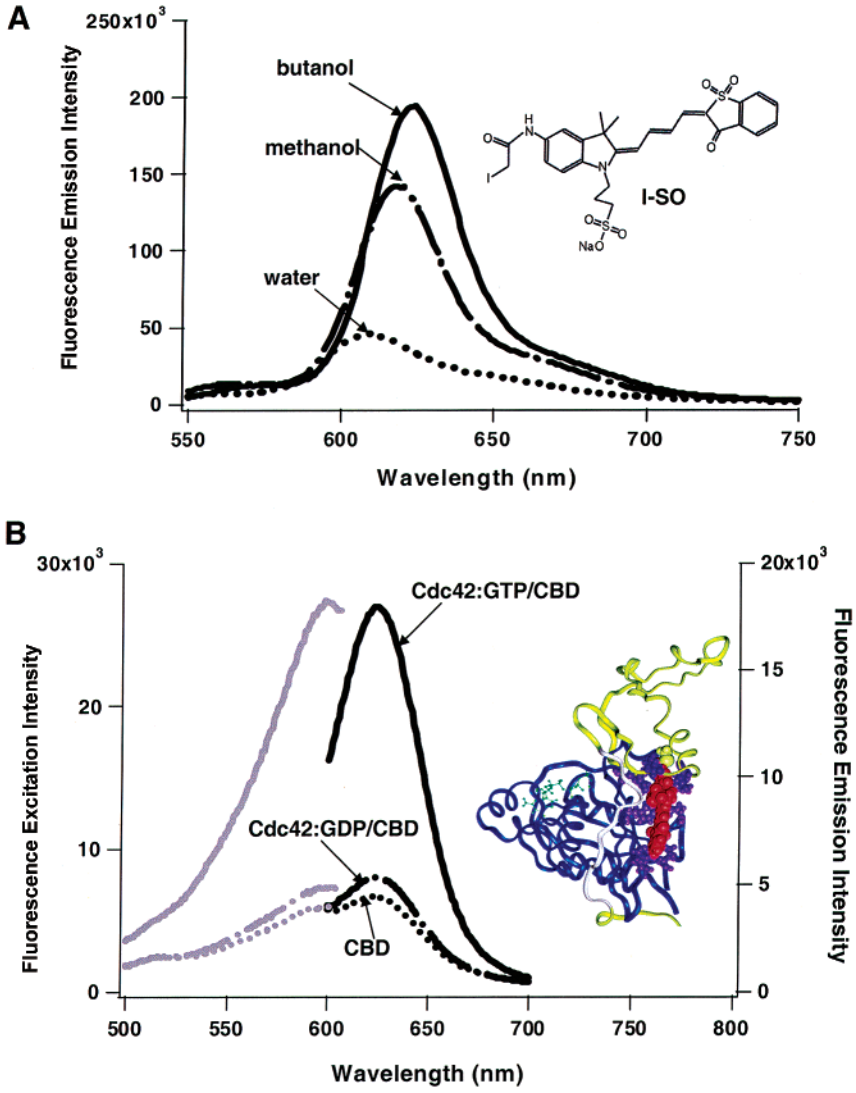

Figure 2. (A) Ensemble fluorescence emission spectra of dye (I−SO) in water (dotted curve), methanol (dashed−dotted curve), and butanol (solid curve). (B) Ensemble fluorescence assays of Cdc42 with CBD biosensor. Fluorescence emission spectra (right side) were obtained with excitation at 568 nm, and fluorescence excitation spectra (left side) were taken with emission at 630 nm. The solid curve pair represents the active GTP-activated Cdc42 forming complexes with dye-labeled CBD; the dash-dotted curve pair represents the GDP-loaded Cdc42 with dye-labeled CBD; and the dotted curve pair represents the dye-labeled CBD alone. A non-hydrolyzable GTP analogue, GTP-γ-S, was used to lock Cdc42 in the active conformation. Inset: a structure based on MD calculations of protein complex Cdc42 (blue)/WASP (yellow) with dye attachment (red) outside the CRIB motif (white) among hydrophobic residues (purple).

hydrophobic residues, to probe relevant Cdc42−CBD interactions while giving minimum perturbation to the protein−protein interactions.

Using single-molecule spectroscopy, we collected fluorescence emission images and trajectories from individual Cdc42−CBD complexes that had been immobilized in agarose gel. Figure 3A displays a raster-scanned fluorescence image (10 μm $\times$ 10 μm) of single-protein complexes. Fluorescence photons were detected by an APD and recorded by a time-stamping TCSPC module. As shown by the top-left plot in Figure 3B, the raw data consist of pairs of registered times for each detected photon, the arrival time (t) and the delay time (Δt), with respect to the laser excitation reference signal.[29] The fluorescence intensity trajectory can be calculated from the histogram of the arrival time t, as shown by the bottom plot in Figure 3B. A nanosecond fluorescence decay curve can be obtained from the histogram of the delay time (Δt) of the fluorescence photons, as shown by the top-right plot in Figure 3B. Therefore, our photon stamping detection was able to record both the fluorescence intensity and the lifetime simultaneously.[29]

From the trajectories of single-protein complexes, we observed fluorescence intensity fluctuations with high to low intensity ratio of more than 3-fold. The fluctuation time scale ranges over 2 orders of magnitude. We have used autocorrelation function to analyze the time scale of the fluctuation. The autocorrelation function, $C(t) = \langle \Delta I(t) \Delta I(0) \rangle / \langle \Delta I(0)^2 \rangle$, is calculated from a single-complex fluorescence intensity trajectory $I(t)$, where $\Delta I(t) = I(t) - \langle I(t) \rangle$. Figure 4A shows an example of the autocorrelation function of a single-complex intensity trajectory. A typical spike at $t = 0$ is due to uncorrelated measurement noise and faster fluctuations beyond the instrument time resolution. For $t > 0$, the autocorrelation function can be fit to a biexponential decay $C(t) = A_f \exp(-k_f t) + A_s \exp(-k_s t)$, with $A_f = 0.17$, $k_f = 250 \pm 60$ s^{-1} and $A_s = 0.14$, $k_s = 45 \pm 10$ s^{-1}. The autocorrelation functions of all single-complex trajectories are fit to either single-exponential or biexponential decays.

On the basis of our control experiments, which indicate that the detectable single-molecule fluorescence only comes from the Cdc42−CBD complex, we attribute the fluorescence

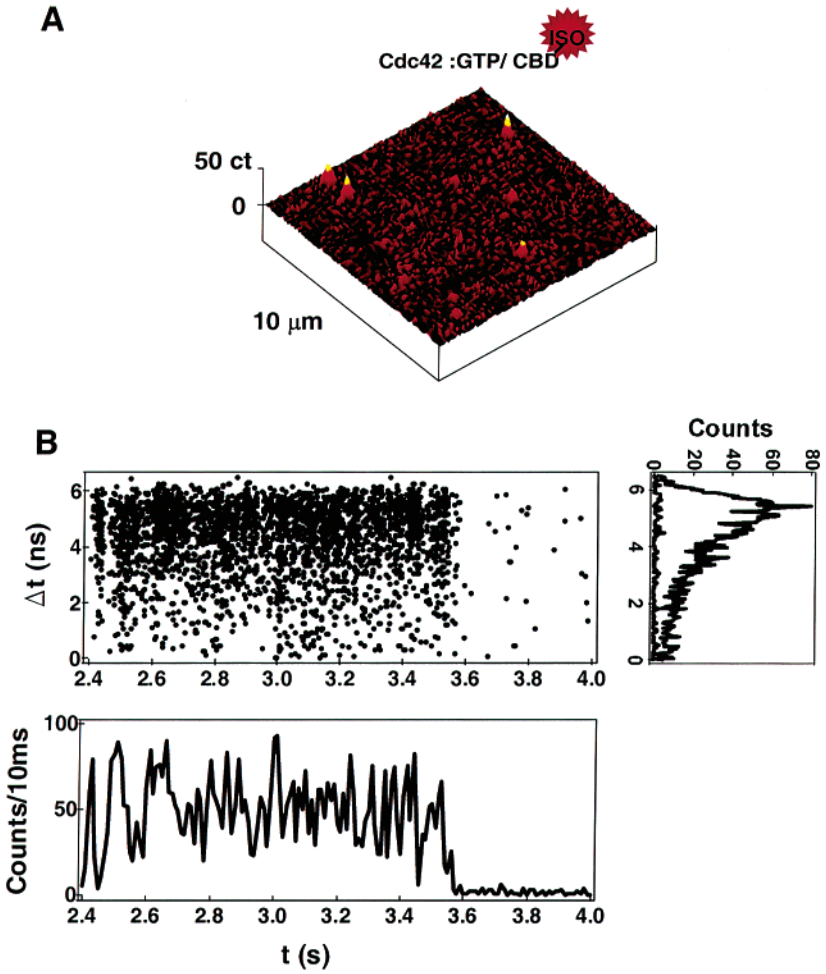

Figure 3. (A) Single-molecule fluorescence raster-scanning image of GTP-loaded Cdc42 in complex with dye-labeled CBD biosensor. (B) Top-left plot is an example of the raw data of one-channel photon time-stamping TCSPC. Each dot corresponds to a photon stamped with an arrival time (t) and a delay time (Δt). The fluorescence intensity trajectory (bottom plot) is calculated from the histogram of the arrival time t with a time-bin resolution of 0.01 s. The dye molecule was photobleached at ~3.6 s. The nanosecond fluorescence decay curves (top-right plot) are the histograms of the delay time (Δt) of the fluorescence photons ($t < 3.6$ s) and background photons ($t > 3.6$ s).

intensity fluctuations to conformational fluctuations of the protein complex. The dissociation constant of activated Cdc42 and the CBD fragment of WASP has been reported[20] in the range of $\sim 10^{-2}$ s^{-1}, suggesting that dissociation of the Cdc42−CBD complex is a rare event during our single-molecule trajectory measurement within a few seconds. This conclusion is consistent with the observation that fluorescence fluctuation was insensitive to the agarose gel concentration (~0.2%−2%), corresponding to the change of cavity sizes (~50−300 nm) of the agarose gel.[16] Subsequent reassociation in the agarose gel should occur within microsecond time scale, considering that the confinement volumes in 0.5% agarose gel are likely <10 pL.[16]

To further confirm that the fluorescence intensity fluctuations are due to protein−protein interactions rather than dye motions or intrinsic photophysical processes, we have studied the intensity trajectories of I−SO dye-labeled CBD alone as a control experiment. CBD alone in buffer solution did not give enough fluorescence intensity for single-molecule measurements, which is consistent with the fact that the I−SO dye is only strongly fluorescent under hydrophobic conditions, as shown in Figure 2A. In an alternative approach, we spin-coated low-concentration CBD on a poly(methyl methacrylate) (PMMA) surface. Less than 20% of the intensity trajectories of CBD on PMMA surface showed fluctuation at rate of ~10 s^{-1}. For the rest of the molecules, the autocorrelation functions have either no other decay components or too small an amplitude, besides the initial shot-noise drop. Those molecules basically have no intensity fluctuations.

To rule out hindered rotation or rotational jumps[36] of the protein complex trapped in the pores of the agarose gel as the origin of the observed intensity fluctuation, we performed single-molecule polarization measurements on individual Cdc42−CBD complexes embedded in agarose gel. The histogram in Figure 5 shows the statistical distribution of the steady-state anisotropy value of the single-protein complex calculated from the single-complex anisotropy trajectory $r(t) = [I_{||}(t) - I_{\perp}(t)]/[I_{||}(t) + 2I_{\perp}(t)]$.[29] The possible value of single-molecule anisotropy is between −0.5 and 1.0, two limiting cases in which the single-molecule transition dipole is either perpendicular or parallel to the linear polarized excitation light. Single molecules with strongly restricted rotational motions show a broad distribution of anisotropy values while freely rotating single molecules show a narrow distribution.[29,37] The protein complexes here show anisotropy values of 0−0.4, with a mean value of ~0.25 (see Figure 5), which indicates free rotation of the protein complex in the agarose gel.

We reached the following conclusions from the control experiments:

(1) The measured conformational fluctuations were spontaneous, because the decay rate constants of the autocorrelation

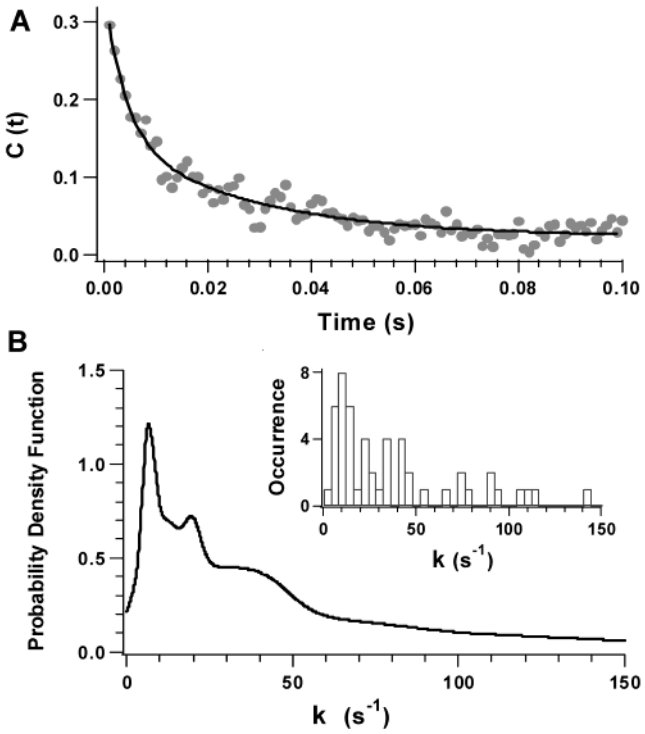

Figure 4. (A) Second-order autocorrelation function, $C(t)$, calculated from a fluorescence intensity trajectory $I(t)$ of a single Cdc42−CBD complex. Solid curve is a biexponential fit with decay rates of 250 ± 60 and 45 ± 10 s^{-1}. (B) The probability density function (PDF) of the conformational fluctuation rates. The PDF is constructed using parameters from fitting the autocorrelation functions for 60 individual protein complexes. Inset: the occurrence histogram of the single-complex conformational fluctuation rate.

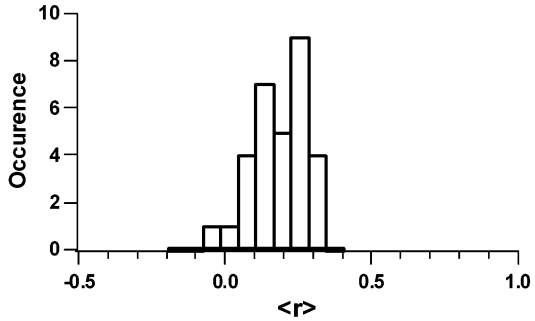

Figure 5. Statistical distribution of the steady-state anisotropy value of single-protein complexes immobilized in agarose gel (0.5%).

functions were independent of the laser excitation intensity at a level of <250 W/cm^2.

(2) Fluorescence fluctuation did not originate from dye interactions in the CBD biosensor, because dye-labeled CBD alone did not give a sufficiently high fluorescence intensity to be detected at the single-molecule level. Only the Cdc42−CBD complex was "visible" to our measurements.

(3) Fluorescence fluctuation was not a result of interaction between the dye-labeled CBD and the agarose gel, because the fluorescence quantum yield of dye-labeled CBD remained as low in the agarose gel as in the buffer solution.

(4) A triplet-state formation of the dye molecule in the Cdc42−CBD complex was unlikely to produce such a fluorescence fluctuation, because the fluctuation is spontaneous rather than photo-induced; besides, the triplet state dynamics would have been at a much faster time scale[38] under ambient conditions than the 10−100-ms time scale observed in our fluorescence intensity fluctuations. The single-molecule control experiments, together with the ensemble-averaged measurements (Figure 2B), support attributing dye fluorescence fluctuations to the protein−protein interactions and the conformational fluctuations at the interface being probed.

Given the location of the dye attachment and the more than 2-fold fluorescence intensity fluctuations, we postulate that the conformational fluctuations involve bound (B) and loosely bound (LB) states of the protein complex. We have reported similar bound and loosely bound states for DNA−protein complexes in a DNA damage recognition system.[16] The LB states are a subset of conformations with deviated nuclear displacements from the bound equilibrium states; they distort the protein−protein interaction interface and the local environment of the dye probe without disrupting the sub-nanometer long-range interactions,[39] so that the overall protein complex is still associated. Compared with the B state, the LB state gives significantly lower fluorescence intensity, as the distorted protein−protein interaction interface probed by the I−SO dye becomes more solvent-accessible and hydrophilic. With respect to our ensemble-averaged assay experiment (Figure 2B), the B state corresponds to the high-intensity Cdc42−CBD bound equilibrium state, where the local environment of the dye probe is much hydrophobic, and the LB state has a hydrophilic local environment of the dye probe resembling the environment of CBD alone. In our single-molecule experiments, fluorescence fluctuations at millisecond and subsecond time scales reflect the Cdc42−CBD conformational changes between the B and LB states.

The conformational fluctuation rates are found to be highly inhomogeneous. The inset in Figure 4B shows an occurrence histogram of fluctuation rate (k). The probability density function (PDF)[40] of the conformational fluctuation rate,

$$\mathrm{PDF}(x) = \sum_i \frac{w_i}{\Delta k_i \sqrt{2\pi}} \exp\left[-\frac{(x-k_i)^2}{2\Delta k_i^2}\right]$$

is constructed using parameters from fitting the autocorrelation functions of single-complex fluorescence intensity trajectories, where k_i, Δk_i, and w_i represent the fluctuation rate, its standard deviation, and its relative weight. The PDF statistically evaluates the rate constants with their standard deviations and occurrences, providing a more reliable distribution than does an occurrence histogram.[40,41] Variations of more than 2 orders of magnitude occur in the conformational fluctuation rates among individual protein complexes, as shown in both panel B of Figure 4 and its inset. Although we are not able to identify exactly how many conformational states contribute to the inhomogeneous distribution, at least two subgroups of states (B_1 and B_2) are associated with conformational fluctuations at ∼10 and ∼40 s^{-1} (see Figure 4B).

Approximately 75% of the single-complex fluorescence intensity trajectories demonstrated single-exponential autocorrelation decays, whereas ∼25% showed biexponential decays, indicating non-Poisson kinetics.[1−7,42] The non-Poisson behavior suggests that the Cdc42−CBD interactions have both static and dynamic inhomogeneities. The dynamic inhomogeneity has been observed for other protein systems[2,13,15−17,43] and may be characterized by the "Agmon−Hopfield" diffusive model[44,45] or the multiple-state Markovian model.[46] Our experimental results, which indicate the existence of at least two subgroup conformations (Figure 4B), can be described qualitatively by a simple two-coupled, two-state Markovian kinetic model

(2×2 model):[46] two slowly interconverting (ζ) conformational fluctuation processes (channel 1 and 2) that have different activation barriers and fluctuation rate constants (k_1, k_1', k_2, k_2').

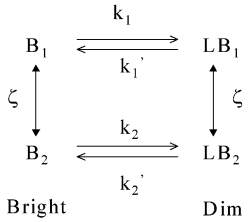

In this 2×2 model, the fluctuation dynamics of each channel is single-exponential with different rate of $\kappa_1 = k_1 + k_1'$ and $\kappa_2 = k_2 + k_2'$. As we have discussed previously, the single-complex conformational fluctuation rate has a broad distribution, and there are primarily two subgroups of rates at $\kappa_1 = 10\ s^{-1}$ and $\kappa_2 = 40\ s^{-1}$ (see Figure 4B). When the interconversion rate (ζ) is comparable to k_1 and k_2, the autocorrelation functions can be biexponential, indicating dynamic inhomogeneity as we have observed for 25% of the single complexes.[1,2,4−7,17] In contrast, for the majority of the individual Cdc42−CBD complexes, the interconversion is either so fast that the autocorrelation function would remain single-exponential according to the Kubo−Anderson line shape theory,[6,47,48] or slower than the measurement time (a few seconds) so that the single-exponential autocorrelation function corresponds to the fluctuation dynamics of either channel 1 or channel 2. At this stage, we are unable to quantitatively measure the interconversion rates or differentiate between conformational fluctuations associated with either very fast or very slow interconversion rates.

We have further explored the possible molecular structure of these multiple conformational states (B_1, B_2, LB_1, and LB_2) using MD simulations. MD simulations are intrinsically single-molecule computational "experiments". The first MD simulation was demonstrated in the late 1970s.[49] For the past 25 years, coupled with extensive knowledge of protein X-ray crystal and NMR structures, MD simulation has become a viable approach to obtain detailed information on protein conformational motions and protein−protein interactions.[50] An important application of MD simulations is to provide a "snapshot" comparison with experimental single-molecule time trajectory. Despite significant effort and progress, combining MD simulations with single-molecule time trajectory is still technically difficult, because of the temporal range mismatch: femtoseconds to nanoseconds (microseconds in few cases)[50−52] for MD simulations limited by computational power, versus sub-milliseconds to seconds for single-molecule spectroscopy limited by excitation saturation and photobleaching. Here, we use MD simulations to explore the interface structures of protein−protein interaction in the dye-labeled Cdc42−CBD complex, which has not been reported previously. The purposes of our MD simulations are (i) to show that the I−SO dye is located in the interacting region of the complex, and it can probe the protein−protein interactions; (ii)

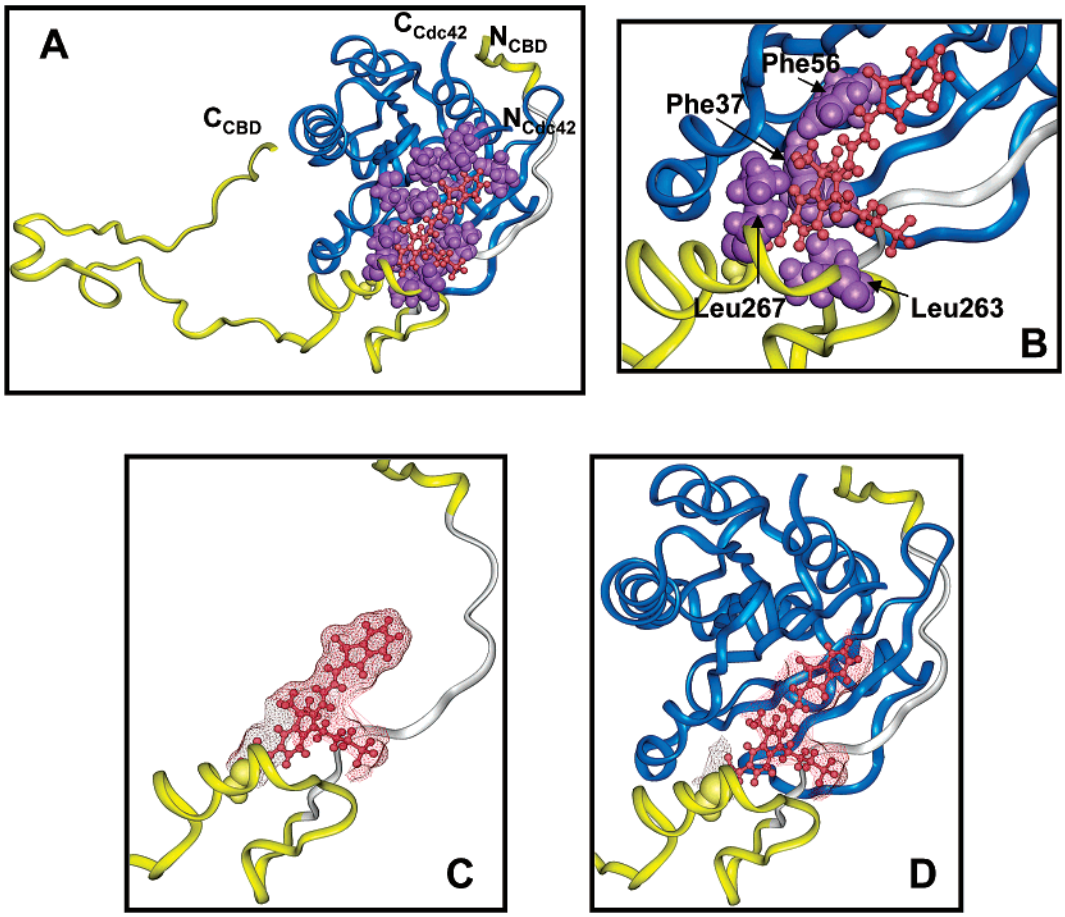

Figure 6. (A) Representative structure of Cdc42 (blue)/CBD (yellow and white) complex based on molecular dynamics (MD) calculations. CPK renderings illustrate the amino acid residues (purple) surrounding the dye molecule (red ball-and-stick). (B) The important hydrophobic interactions involving Cdc42 Phe37 and Phe56 and WASP Leu263 and Leu267 that were probed by the dye molecule. (C) Solvent-accessible surface (mesh rendering) of the dye molecule prior to binding of CBD to Cdc42; the surface area was ~377 Å^2. (D) Solvent-accessible surface of the dye molecule after Cdc42−CBD binding; the surface area reduced to ~225 Å^2.

to show that the characteristic interacting region of Cdc42 and CBD is not drastically changed by the dye attachment; (iii) to estimate the protein−protein interaction interface for B and LB states of the Cdc42−CBD complex; and (iv) to enhance our understanding of the LB states.

For MD simulations of the Cdc42−CBD complex, we obtained the NMR structures of Cdc42 in complex with a WASP fragment from the Protein Data Bank. Based on model 5 of 1CEE (20 NMR-derived solution structures of Cdc42 in complex with the WASP fragment),[19] we attached the dye molecule and extended the WASP C-terminal segment, according to the structure of our CBD biosensor. After energy minimization using a molecular mechanics CVFF force field,[32,33] a trajectory of 10 ps as a "snapshot" was calculated with a distance-dependent dielectric constant under the condition of no surrounding water molecules.

A representative complex of Cdc42 (blue) and CBD (yellow) is shown in Figure 6A. The solvatochromic dye was located within the protein interfacial pocket. Among amino acid residues (purple) surrounding the dye molecule (red) were Cdc42 Phe37 and Phe56 residues and WASP Leu263 and Leu267 residues, as shown in Figure 6B. These residues formed important hydrophobic contacts; disruption of these contacts through mutation or elimination leads to significant decrease in the binding affinity of Cdc42/WASP.[19] The MD calculations further confirmed that the dye molecule probed important hydrophobic interactions outside the conserved binding motif CRIB (white). Various modes of interactive motions, especially those involving the important hydrophobic residues (Cdc42 Phe37 and Phe56 and WASP Leu263 and Leu267), could result in multiple conformations between B and LB states, whereas the overall complex is still associated. The rate distribution in Figure 4B reflects this conformational inhomogeneity and the fluctuations. Because the dye fluorescence properties are sensitive to the local environment, conformational fluctuations in the probed signaling region lead to dye fluorescence fluctuations observed in the single-molecule experiments.

Figures 6C and 6D demonstrate that the solvent-accessible surface area of the dye molecule undergoes a decrease from ~377 Å^2 to ~225 Å^2 upon Cdc42−CBD binding. This signifies an increasingly hydrophobic environment that surrounds the dye molecule upon formation of the protein complex, which is consistent with ensemble fluorescence measurements (see Figure 2). It is likely that the B and LB conformational states correspond to different degrees of distortion of the solvent-accessible surface and that the LB states are more solvent-accessible.

MD simulations can provide a "snapshot" assessment of possible conformational structures, and this approach is particularly informative when the results can be evaluated considering the single-molecule spectroscopic experiments. However, it is still difficult to determine the specific molecular configurations of residue interactions that various conformational states might constitute. Similar single-molecule measurements of protein complexes with point mutations in the probed signaling region might illuminate the issue; however, mutations in this region could disrupt Cdc42/WASP recognition.[20] Although more-sophisticated MD simulations that consider water molecules and counterions may provide more accurate structural and energetic characterizations, our MD simulations shed light on essential conformations of the multiple states involved in Cdc42−CBD interaction dynamics.

Conclusions

We have conducted a single-molecule study of protein−protein interaction dynamics in an intracellular signaling protein complex, Cdc42/WASP. Using a novel CBD biosensor, which is a dye-labeled WASP fragment that binds only the GTP-activated Cdc42, we were able to probe hydrophobic interactions significant to Cdc42/WASP recognition. Single-molecule fluorescence measurements revealed static and dynamic inhomogeneities in this protein−protein interaction dynamics, and our study characterized the dynamic nature of molecular recognition within the Cdc42/WASP signaling complex. A coupled-two channel Markovian model was proposed for the fluctuation dynamics of protein−protein interactions, and the possible molecular structures of the protein complex were explored by molecular dynamics (MD) simulations.

The Cdc42−CBD complexes showed conformational fluctuations between bound and loosely bound states while the overall complex was still associated. The distribution of the fluctuation rates was highly inhomogeneous with variations of 2 orders of magnitude among individual complexes under the same condition, indicating static inhomogeneous dynamics. The conformational fluctuation dynamics of ~25% of the single complexes also showed dynamic inhomogeneity, i.e., rate changes during the measurements of protein−protein interactions. The results suggest highly dynamic rather than static protein−protein interactions in this cell signaling system. By establishing a molecular imaging system with adequate spatial and temporal resolution and combining single-molecule experimental and computational approaches, we expect to expand our studies to other important biomolecular complexes under physiological conditions and eventually to living cells.

Acknowledgment. This work was supported by the Laboratory Directed Research and Development Program of Pacific Northwest National Laboratory, operated for the U.S. Department of Energy by Battelle Memorial Institute (X.T., D.H., E.R.V., and H.P.L.), the National Institutes of Health (K.M.H.), Deutsche Forschungsgemeinschaft (P.N.), and the Leukemia and Lymphoma Society (A.T.).

References and Notes

(1) Zwanzig, R. *Acc. Chem. Res.* **1990**, *23*, 148.
(2) Frauenfelder, H.; Sligar, S. G.; Wolynes, P. G. *Science* **1991**, *254*, 1598.
(3) Wang, J.; Wolynes, P. *Phys. Rev. Lett.* **1995**, *74*, 4317.
(4) Geva, E.; Skinner, J. L. *Chem. Phys. Lett.* **1998**, *288*, 225.
(5) Yang, S. L.; Cao, J. S. *J. Phys. Chem. B* **2001**, *105*, 6536.
(6) Xie, X. S. *J. Chem. Phys.* **2002**, *117*, 11024.
(7) Jung, Y. J.; Barkai, E.; Silbey, R. J. *J. Chem. Phys.* **2002**, *117*, 10980.
(8) Papoian, G. A.; Ulander, J.; Wolynes, P. G. *J. Am. Chem. Soc.* **2003**, *125*, 9170.
(9) Iakoucheva, L. M.; Walker, R. K.; van Houten, B.; Ackerman, E. J. *Biochemistry* **2002**, *41*, 131.
(10) Weiss, S. *Science* **1999**, *283*, 1676.
(11) Moerner, W. E.; Orrit, M. *Science* **1999**, *283*, 1670.
(12) Mehta, A. D.; Rief, M.; Spudich, J. A.; Smith, D. A.; Simmons, R. M. *Science* **1999**, *283*, 1689.
(13) Weiss, S. *Nat. Struct. Biol.* **2000**, *7*, 724.
(14) Wazawa, T.; Ishii, Y.; Funatsu, T.; Yanagida, T. *Biophys. J.* **2000**, *78*, 1561.
(15) Lu, H. P.; Xun, L. Y.; Xie, X. S. *Science* **1998**, *282*, 1877.
(16) Lu, H. P.; Iakoucheva, L. M.; Ackerman, E. J. *J. Am. Chem. Soc.* **2001**, *123*, 9184.
(17) Edman, L.; Rigler, R. *Proc. Natl. Acad. Sci. U.S.A.* **2000**, *97*, 8266.
(18) Zhuang, X. W.; Bartley, L. E.; Babcock, H. P.; Russell, R.; Ha, T. J.; Herschlag, D.; Chu, S. *Science* **2000**, *288*, 2048.

(19) Abdul-Manan, N.; Aghazadeh, B.; Liu, G. A.; Majumdar, A.; Ouerfelli, O.; Siminovitch, K. A.; Rosen, M. K. *Nature* **1999**, *399*, 379.
(20) Rudolph, M. G.; Bayer, P.; Abo, A.; Kuhlmann, J.; Vetter, I. R.; Wittinghofer, A. *J. Biol. Chem.* **1998**, *273*, 18067.
(21) Erickson, J. W.; Cerione, R. A. *Curr. Opin. Cell Biol.* **2001**, *13*, 153.
(22) Johnson, D. I. *Microbiol. Mol. Biol. Rev.* **1999**, *63*, 54.
(23) Kim, A. S.; Kakalis, L. T.; Abdul-Manan, M.; Liu, G. A.; Rosen, M. K. *Nature* **2000**, *404*, 151.
(24) Rudolph, M. G.; Linnemann, T.; Grunewald, P.; Wittinghofer, A.; Vetter, I. R.; Herrmann, C. *J. Biol. Chem.* **2001**, *276*, 23914.
(25) Nomanbhoy, T.; Cerione, R. A. *Biochemistry* **1999**, *38*, 15878.
(26) Kraynov, V. S.; Chamberlain, C.; Bokoch, G. M.; Schwartz, M. A.; Slabaugh, S.; Hahn, K. M. *Science* **2000**, *290*, 333.
(27) Toutchkine, A.; Kraynov, V.; Hahn, K. *J. Am. Chem. Soc.* **2003**, *125*, 4132.
(28) Hahn, K.; Toutchkine, A. *Curr. Opin. Cell Biol.* **2002**, *14*, 167.
(29) Hu, D. H.; Lu, H. P. *J. Phys. Chem. B* **2003**, *107*, 618.
(30) Bohmer, M.; Pampaloni, F.; Wahl, M.; Rahn, H.; Erdmann, R.; Enderlein, J. *Rev. Sci. Instrum.* **2001**, *72*, 4145.
(31) Fries, J. R.; Brand, L.; Eggeling, C.; Köllner, M.; Seidel, C. A. M. *J. Phys. Chem. A* **1998**, *102*, 6601.
(32) Wang, W.; Donini, O.; Reyes, C. M.; Kollman, P. A. *Annu. Rev. Biophys. Biomol. Struct.* **2001**, *30*, 211.
(33) Ewig, C. S.; Thacher, T. S.; Hagler, A. T. *J. Phys. Chem. B* **1999**, *103*, 6998.
(34) Sagui, C.; Darden, T. A. *Annu. Rev. Biophys. Biomol. Struct.* **1999**, *28*, 155.
(35) Hoffman, G. R.; Cerione, R. A. *Cell* **2000**, *102*, 403.
(36) Ha, T.; Glass, J.; Enderle, T.; Chemla, D. S.; Weiss, S. *Phys. Rev. Lett.* **1998**, *80*, 2093.
(37) Ha, T.; Laurence, T. A.; Chemla, D. S.; Weiss, S. *J. Phys. Chem. B* **1999**, *103*, 6839.
(38) English, D. S.; Furube, A.; Barbara, P. F. *Chem. Phys. Lett.* **2000**, *324*, 15.
(39) Shoemaker, B. A.; Portman, J. J.; Wolynes, P. G. *Proc. Natl. Acad. Sci. U.S.A.* **2000**, *97*, 8868.
(40) Schmidt, T.; Schutz, G. J.; Baumgartner, W.; Gruber, H. J.; Schindler, H. *J. Phys. Chem.* **1995**, *99*, 17662.
(41) Harms, G. S.; Orr, G.; Montal, M.; Thrall, B. D.; Colson, S. D.; Lu, H. P. *Biophys. J.* **2003**, *85*, 1826.
(42) Barsegov, V.; Chernyak, V.; Mukamel, S. *J. Chem. Phys.* **2002**, *116*, 4240.
(43) Ha, T. J.; Ting, A. Y.; Liang, J.; Caldwell, W. B.; Deniz, A. A.; Chemla, D. S.; Schultz, P. G.; Weiss, S. *Proc. Natl. Acad. Sci. U.S.A.* **1999**, *96*, 893.
(44) Agmon, N. *J. Phys. Chem. B* **2000**, *104*, 7830.
(45) Agmon, N.; Hopfield, J. J. *J. Chem. Phys.* **1983**, *78*, 6947.
(46) Schenter, G. K.; Lu, H. P.; Xie, X. S. *J. Phys. Chem. A* **1999**, *103*, 10477.
(47) Anderson, P. W. *J. Phys. Soc. Jpn.* **1954**, *9*, 316.
(48) Kubo, R. *Fluctuation, Relaxation, and Resonance in Magnetic Systems*; Oliver and Boyd: London, 1961.
(49) McCammon, J. A.; Karplus, M. *Nature* **1977**, *267*, 585.
(50) Karplus, M.; McCammon, J. A. *Nat. Struct. Biol.* **2002**, *9*, 646.
(51) Daggett, V. *Curr. Opin. Struct. Biol.* **2000**, *10*, 160.
(52) Duan, Y.; Kollman, P. A. *Science* **1998**, *282*, 740.